Archives of Hygiene Sciences
Qom University of Medical Sciences
Summer 2021. Volume 10. Number 3

Research Paper:
Photo-catalytic Ozonation for Degrading Terephthalic Acid in Aqueous Environment

Kazem Mahanpoor[1*], **Zahra Sharifnezhad**[1]

1. Department of Chemistry, Arak Branch, Islamic Azad University, Arak, Iran.

Use your device to scan and read the article online

Please cite this article as Mahanpoor K, Sharifnezhad Z. Photo-catalytic Ozonation for Degrading Terephthalic Acid in Aqueous Environment. Archives of Hygiene Sciences. 2021; 10(3):201-214. http://dx.doi.org/10.32598/AHS.10.3.201

http://dx.doi.org/10.32598/AHS.10.3.201

Article info:
Received: 12 Nov 2021
Accepted: 03 Apr 2021
Publish: 01 Jul 2021

Keywords:
Terephetalic acid (TPA), Fluidized-Bed, Advanced oxidation, Full factorial, Decomposition

ABSTRACT

Background & Aims of the Study: Terfetalic Acid (TPA) is produced in large quantities and used in various industries. Besides, TPA is among the main sources of water pollution in industrialized countries. TPA photo-degradation process was performed in a Circulating Fluidized Bed Reactor (CFBR) by one Ultraviolet type A (UV-A) lamp and ozone generator with $MnFe_2O_4$/Willemite photo-catalyst.

Materials and Methods: In this research, the nanoparticles of $MnFe_2O_4$ and Willemite were synthesized by co-precipitation reactions and wet mixing method, respectively. Then $MnFe_2O_4$/Willemite was synthesized by the immobilization of $MnFe_2O_4$ on Willemite by mechanical method. Full factorial experimental design with 4 factors, including the pH, the initial concentration of TPA, the amount of Catalyst (Cat.), and O_3 dosage was used for modeling and optimizing the process.

Results: In the optimal conditions, the amounts of pH, TPA, Cat., and O_3 were obtained equal to 9, 20 ppm, 1.5 g/L, and 2.17 mg/h, respectively. In these conditions, degradation efficiency was obtained to be 98.2695%, and decomposition kinetics was determined as pseudo-first-order with K_{app}=0.2707 min^{-1}, k_{LH}=3.729 ppm min^{-1}, and k_{add}=0.051 ppm^{-1}.

Conclusion: Comparing experiments results in different processes, such as UV, UV-Cat, O_3, UV-O_3, Cat-O_3, and UV-Cat-O_3 revealed that photo-catalytic ozonation (O_3/$MnFe_2O_4$/Willemite) in the presence of UV for degradation of TPA in an aqueous environment, present the higher efficiency.

* **Corresponding Author:**
Kazem Mahanpoor, PhD.
Address: *Department of Chemistry, Arak Branch, Islamic Azad University, Arak, Iran.*
Phone: *+98 (86) 33412608*
E-mail: *k-mahanpoor@iau-arak.ac.ir*

Archives of Hygiene Sciences
Qom University of Medical Sciences

1. Introduction

Supplying drinking water, energy, and food are the major future challenges; more importantly, water significantly influences the quality and quantity of energy, environment, and food [1]. Aromatic organic compounds, like Terephthalic Acid (TPA), are produced in high volume and are among the main sources of water pollution in industrialized countries.

TPA is widely used in numerous industries for producing polymers, such as Polyethylene Terephthalate (PET), polybutylene terephthalate, polyester, and polyamide [2]. Additionally, it is used for producing carriers in paint, plasticizer, drug, metal-organic framework, filler in some military smoke grenades, as well as deuterated terephthalate and related polymer [3, 4]. Due to the very large-scale production of this substance in the world, there is always some of this substance in the environment. Moreover, according to research, this substance presents carcinogenic properties in rats [5] and reproductive toxicity in male mice [6].

There exist numerous methods to remove pollutants from water and wastewater, such as coagulation and flocculation, filtration, biological purification by microorganisms, reverse osmosis, Electro-Dialysis Reverse (EDR), ion exchange resins, adsorption, evaporation, and Advanced Oxidation Processes (AOP) [7-9]. Researchers found that each of these methods has disadvantages and advantages [7-9]. Implementing Advanced Nanoparticles (NPs) in AOP provides special opportunities for the recovery of wastewater. Specifications, such as the elimination of trace, toxic contaminants, microbial pathogens, resistant pollutants, the conversion of the wide range of organic materials to carbon dioxide and water, the low cost of equipment, the high rate of reactions, less energy consumption, and less human toxicity are benefits, i.e., likely to result from AOP [7, 10]. Additionally, what has motivated the researchers to choose the AOP method is the ability of photo-catalyst to integrate the NPs with multifunction water purification systems. Moreover, using NPs has been developed in the field of water treatment [11].

Therefore, $MnFe_2O_4$ was applied as the main catalyst to exploit its properties. The $MnFe_2O_4$ was immobilized on a base to increase the specific surface area, raise the strength of the catalyst, facilitate its separation on large scale, reuse the catalyst, and reduce the cost of the operation [11, 12]. Therefore, Willemite was selected as the basis, because of its excellent chemical and thermal stability, water resistance, and cost-effectiveness [13].

Statistical design techniques may be used to model and optimize the process. In the statistical design experiments, the factors involved in tests at their respective levels were simultaneously varied. One of the most widely used experimental design techniques is the full factorial method; this approach simultaneously investigates the effect of more than one factor in the response. Two-level full factorial designs of experiments are the most common patterns in which each factor is experimentally tested for only two levels [14].

Therefore, in this research, the degradation of TPA, as an aromatic pollutant was investigated by O_3/$MnFe_2O_4$/Willemite, as photo-catalytic ozonation under the UV Irradiation process. The effects of pH, the initial concentration of TPA, the amount of catalyst, and O_3 dosage for higher degradation of TPA were investigated using a full factorial experimental design. Additionally, a kinetic study was developed using the experimental results attained in this investigation.

Numerous studies have been accomplished to eliminate TPA (Table 1) by photo-catalysts, such as TiO_2, Fe, ZnO, and TiO_2/AC [3, 15-21]. The process of removing contaminants by these photo-catalysts is not only time-consuming but also the mineralization of TPA and intermediates fail to occur absolutely. Furthermore, catalyst separation is a difficult task. The magnetic properties of $MnFe_2O_4$/Willemite allow the photo-catalyst to be separated and retrieved. It has certain characteristics, such as chemical stability, low cost, and very low bandgap energy [12].

In this study, the TPA removal process was examined by photo-catalytic methods ($MnFe_2O_4$/Willemite) in a Circulating Fluidized Bed Reactor (CFBR) by one UV-A lamp and ozone generator. To compare different processes, the TPA degradation experiments were performed by UV, UV-Cat., O_3, UV-O_3, Cat.-O_3, and UV-Cat.-O_3, separately. Full factorial experimental design with 4 factors was used for modeling and optimizing the process. In the optimal conditions, the amounts of pH, TPA, Cat., and O_3 were obtained. The relevant results suggested that the UV-Cat.-O_3 process has higher efficiency. Finally, the kinetic and reproducibility of photo-catalytic was considered in optimum conditions.

2. Materials and Methods

Most required chemical reagents were provided from Sigma Aldrich and Merck Company. Agilent 8453 UV-visible

Table 1. Some studies to remove TPA by the kind of catalyst

Photo-catalyst	Synthesis Method	Condition	Degradation Efficiency	Ref.
UV–TiO_2; UV–H_2O_2; UV–H_2O_2–Fe; O_3; O_3/Fe; O_3/TiO_2; UV-O_3-H_2O_2-Fe; UV-O_3-H_2O_2-Fe-TiO_2	Commercial	Terephthalic acid (ppm): 50; H_2O_2 (mM): 3; $Fe_2(SO_4)3$ Conc. (mg/L): 90; Cat. amount (mg/L): 1000; Particle size (nm): 20±5 nm; particles surface area (m^2 g^{-1}): 50±15; pH: 8; Temp.(°C): ambient temperature; removal time (min): 600 in UV–TiO_2 system, to <10 by UV-H_2O_2-Fe-O_3 system; kinetic model: pseudo-first order; irradiation source: six quartz tube mercury vapor (40W); irradiation intensity (μW/cm^2): 144; wavelength (nm): 253.7; the amount of ozone (mg/h): 2.4	UV-TiO_2< UV-H_2O_2< UV-H_2O_2-Fe(III)< O_3 < O_3-Fe(III)< O_3-TiO_2< UV-H_2O_2-Fe(III)-TiO_2-O_3≤ UV-H_2O_2-Fe-O_3	[3]
UV-H_2O_2-Fe	-	Terephthalic acid (ppm): 28.450; H_2O_2 (mM): 20; $FeSO_4$(g/L): 1; pH: 9; removal time (min): 40; irradiation source: six UV light (Phillips, tube mercury vapor lamps, 40 W); irradiation intensity (μW/cm2): 144; wavelength (nm): 253.7	60	[15]
UV-O_3-Fe		Terephthalic acid (ppm): 28.450; $FeSO_4$(g/L): 1; removal time (min): 10; irradiation source: six UV light (Phillips, tube mercury vapor lamps, 40 W); irradiation intensity (μW/cm^2): 144; wavelength (nm): 253.7	95	
UV-O_3-H_2O_2-Fe		Terephthalic acid (ppm): 28.450; removal time (min): 30; irradiation source: six UV light (Phillips, quartz tube mercury vapor ultraviolet lamps, 40 W); irradiation intensity (μW/cm^2): 144; wavelength (nm): 253.7; the amount of ozone (g/hr): 2.4	-	
SO_4^{2-}/TiO_2; bare TiO_2; P25	Sol-gel - Commercial	The aqueous solution of phthalic acid (ppm): 38.2; Cat. amount (%): 1.38; particle size (nm): 12, 25 (for SO_4^{2-}/TiO_2 & bare TiO_2); pH: 9; Temp.(°C): 25±2; removal time (min):120; kinetic model: pseudo-first order; K (min^{-1}): 0.072 (for initial [TA]: 38.2 ppm & 3.79% SO_4^{2-}/TiO_2); irradiation source: UVP mercury lamp B-100AP/R (100 W); irradiation intensity (μW/cm^2): 18	SO_4^{2-}/TiO_2 ~ bare TiO_2 ~ P25	[16]
O_3; O_3-LEDs; O_3-ZnO; O_3-V_xO_y/ZnO; O_3-V_xO_y/ZnO-LEDs		Terephthalic acid (mg/L): 30; Cat. amount (gr/L): 0.1; Particle size (nm): 41; particles surface area (m^2 g^{-1}): 8.60; pH: without pH; Temp.(°C): 25; removal time (min): 60; K (min^{-1}):0.0512, 0.0565, 0.0523, 0.0656, 0.0644, 0.628 in ozone, O_3-LEDs, O_3-ZnO , O_3-VxOy/ZnO, O_3-VxOy/ZnO-LEDs, respectively; irradiation source: six UV light (Phillips, quartz tube mercury vapor ultraviolet lamps, 40 W); irradiation intensity (μW/cm^2): 144; wavelength (nm): 253.7; the amount of ozone(g/hr): 2.4; rector: double-vessel Pyrex semi-batch reactor (2 L)	32% (for O_3); 40% (for O_3-UVAs); 64% (for O_3-ZnO); 74% (for O_3-V_xO_y/ZnO) 98% (for O3-VxOy/ZnO-UVA)	[17]
TiO_2; ZnO	Commercial	Terephthalic acid (ppm): 20-100; Cat. amount (gr/L): 2.5; particle size (nm): 21 & 100 for TiO_2 & ZnO; particles surface area (m^2 g^{-1}): 50±15, 13.01 for TiO_2 & ZnO; pH: 6 and 9 for TiO_2 and ZnO; H_2O_2 (mmol/L):5.4; Temp.(°C): 25-30; removal time (min): 30; kinetic model: pseudo-first order; K (min^{-1}):0.124 & 0.1001 for TiO_2 and ZnO; KLH (ppm/min):2.582 & 3.176 for TiO_2 & ZnO; irradiation source: eight quartz tube mercury vapor lamps; irradiation intensity (μW/cm^2): 21; wavelength (nm): 253.7; Reactor: double-walled Pyrex batch cylindrical (1.5 L)	42% (for TiO_2) 62% (for ZnO)	[18]
TiO_2/AC	Sol-gel	Terephthalic acid (ppm): 6 g/L; Cat. amount (gr/L): 7 ; particle size (nm): 17.6; particles surface area (m^2 g^{-1}): 887.11; Temp.(°C): room temp.; Removal time (h): 8; irradiation source: UV lamp (20 W); wavelength (nm): 253.7	64.3%	[19]
Photolysis; O_3; O_3-V_xO_y/TiO_2; O_3-V_xO_y/TiO_2-LED	Impregnation	Terephthalic acid (g/L): 30; Cat. amount (gr/L): 0.1 ; Temp.(°C): 25; removal time (min): 60; Kinetic model: pseudo-first order; irradiation source: LEDs and UV lamp (4 W m^{-2}); wavelength (nm): 380–430 nm & 365–465 (for LED & UV lamp); the amount of ozone(mg/L): 10; reactor: double-vessel Pyrex semibatch cylindrical (2.0 L)	O_3-V_xO_y/TiO_2> O_3-V_xO_y/TiO_2-LED> O_3 > O_3-V_xO_y/TiO_2-UV> O_3- TiO_2> O_3-TiO_2-LED	[20]
TiO_2	Hydrolysis of $TiCl_4$ in a highly acidic media	Terephthalic acid (ppm): 20; Cat. amount (g/L): 0.75; particle size (nm): 6.8; pH: 3.7; Temp.(°C): 25; removal time (min):180; kinetic model: pseudo-first order; K (min^{-1}): 0.0336; irradiation source: visible light; reactor: double-walled borosilicate cylindrical batch reactor.	99	[21]

Table 2. The structure and characteristics of TPA

Item	Information
Pollutant	Para-Terephthalic Acid (TPA)
Structure	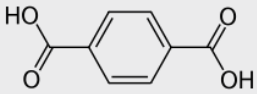
λ_{max} (nm)	240
Molecular weight (g.mol^{-1})	166.132

Archives of Hygiene Sciences
Qom University of Medical Sciences

spectrophotometer was employed to appoint the presence of TPA in a sample and the percentage of degradation in aqueous media. In the degradation pollutant process, one UV-A lamp with a power of 15 W and ozone generator was obtained from Philips and Nabbzist Company (Iran), respectively. The decomposition of TPA was performed in a Circulating Fluidized Bed Reactor (CFBR) with rotary current and an effective volume of 1 liter. The structure and chemical properties of TPA are illustrated in Table 2.

The process of photocatalytic decomposition of TPA was performed by Circulating Fluidized Bed Reactor (CFBR) with rotary current and effective volume of 1 liter (Figure 1). One UV-A lamp with a power of 15 W (Philips) was directly placed in the reactor so that the liquid flow revolves around the lamp. This reactor was continuous for ozone and batch for $MnFe_2O_4$/Willemite and TPA. An ozone generator from Nabbzist Company (Iran) was used in this process. A pressure capsule was applied to produce the pure oxygen for passing in the ozone generator. The photo-reactor was developed with a water-flow jacket joined to a Thermo-Bath (ALB64 model, FINEPCR Korean Company) for controlling the temperature at 25ºC in all experiments. The pH was measured by pH meter F-71 HORIBA (Germany).

Catalyst preparation

The preparation of Willemite was performed according to previous research [13, 22]. Therefore, 0.1 moles of ($ZnSO_4.7H_2O$) was dissolved in 100 mL of deionized water. NaOH solution (0.2 moles NaOH/100ml H_2O) was added drop-wise to zinc sulfate solution and stirred at 80°C. The solution was gradually cooled to ambient temperature. The precipitated $Zn(OH)_2$ was separated from the solution by centrifugation and dried at 100°C for 12 h. Moreover, 2 moles of $Zn(OH)_2$ and 1 mole of silica high purity powder were added to 200 mL water and stirred at 80°C for 4 h. Finally, the precipitate was separated by centrifuge, dried at 80°C, and calcined at 1050°C (Figure 2).

Based on previous research [23, 24], 0.2 moles of ($Fe(NO_3)_3.9H_2O$) and 0.1 moles of ($Mn(NO_3)_2.4H_2O$) were completely dissolved in the 200 mL of distilled water. Then, urea solution (0.4 moles of urea in 250 mL water), as the precipitating agent, was added to the solution containing iron nitrate and manganese nitrate, drop

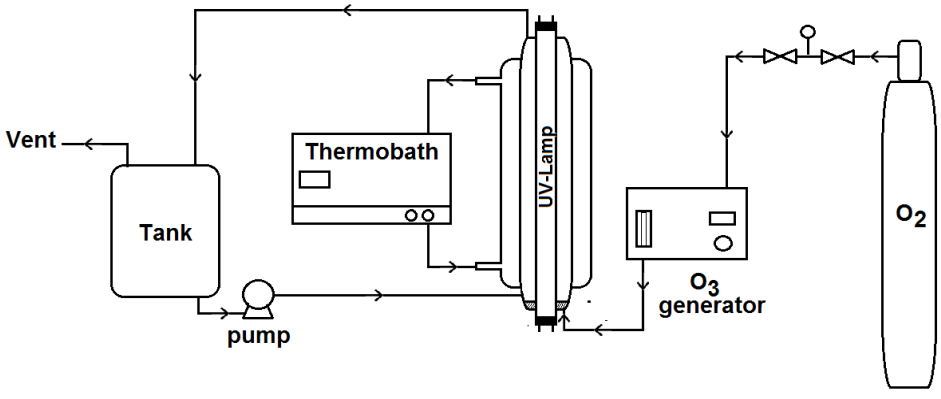

Figure 1. The experimental set-up

Archives of Hygiene Sciences
Qom University of Medical Sciences

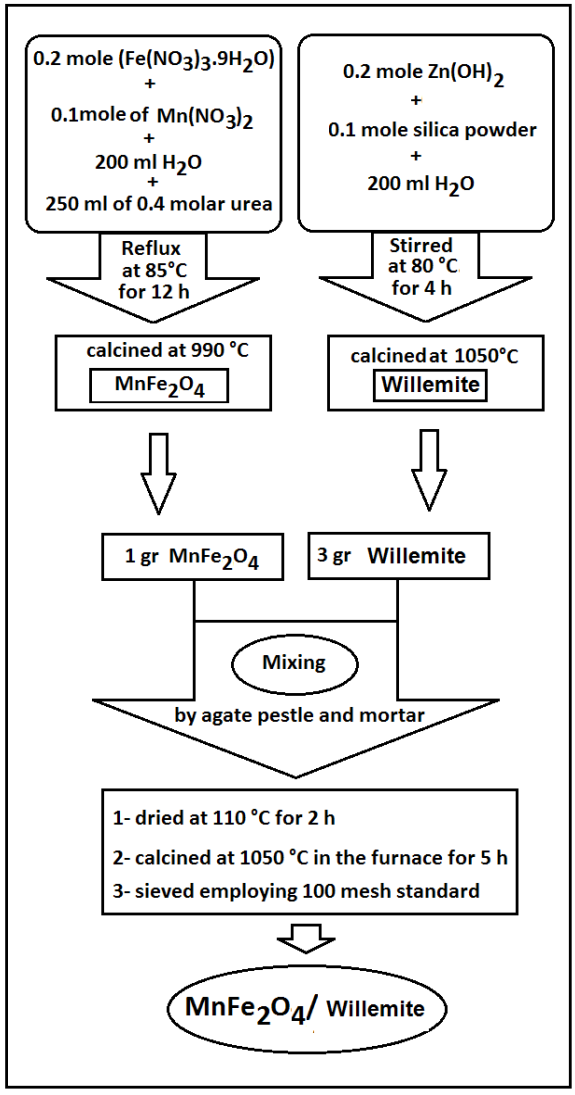

Figure 2. The process of catalysts synthesis

by drop. The total solution was refluxed at 85°C for 12 h. After the gradual cooling of the contents, the precipitate was separated by centrifuge and washed by water and ethanol. Precipitates were dried in the oven at 80°C and calcined in the furnace at 990°C. The main photo-catalyst was synthesized by mixing $MnFe_2O_4$ and Willemite (1:3 w/w %) in the presence of ethanol using agate pestle and mortar. Next, this mixture was dried at 110°C in an oven for 2 h and calcined at 1050°C in the furnace for 5 h. The precipitation was sieved applying a 100 mesh standard sieve (Figure 2).

The experimental design was used to study the effects of simultaneously changing the values of variables on the removal of TPA from an aqueous solution. Additionally, the main factor influencing the process, the interaction manner of variables on each other, and the percentage of removal of TPA were determined by the experimental design method.

The designed experiment was created in Minitab 17 using a full factorial design [14]. Operational factors, containing an initial TPA concentration, ozone dosage, the amount of photo-catalyst, and pH are presented in Table 3. Operation factors and factor levels being influential on the response of the TPA degradation were confirmed by primary experiments. Other parameters, such as temperature, light wavelength, light intensity, and stirring rate were constant in the process. Corresponding to Equation 1, nineteenth runs (N) were designed based on 4 factors (k), 2 of factor levels, 3 of center points (C0), and without replicates of the corner points (r).

(1) $N=r\times(level)^k+C_0$

The randomization technique was selected to balance the effect of irrelevant or uncontrollable conditions and estimate the intrinsic variation. Besides, DOE was performed by coding factors corresponding to the design matrix.

Based on experimental data, there were significant relationships between the response (TPA degradation) and 4 input factors (Equation 2). New results will easily predict based on mathematical Equation 2.

(2) $Y=\beta_0+\beta_1A+\beta_2B+\beta_3C+\beta_4D+\beta_{12}AB+\beta_{13}AC+\beta_{14}AD+\beta_{23}BC+\beta_{24}BD+\beta_{34}CD+\beta_{123}ABX+\beta_{124}ABD+\beta_{134}ACD+\beta_{234}BCD+\beta I_{234}ABCD+\varepsilon$

Where $ß_0$ is overall mean, $ß_1$, $ß_2$, $ß_3$, and $ß_4$ are linear coefficients, $ß_{12}$, $ß_{13}$, $ß_{14}$, $ß_{23}$, $ß_{24}$, $ß_{34}$, $ß1_{23}$, $ß_{123}$, $ß_{124}$, $ß_{134}$, $ß_{234}$, and $ß_{1234}$ are interactions coefficients, and ε is random error or noise. The Analysis of Variance (ANOVA) was performed by the consideration of P-value related to the Adjusted Mean Square (Adj. MS) of the main factors, the Adj. MS of interacting factors, total Adj. MS, error Adj. MS, model Adj. MS, and the inspection of the standard deviation of the residuals (S), R Square (R^2), Adjusted R Square (Adj. R^2) and Predicted R Square (Pred. R^2) values.

A regression analysis model was simplified by eliminating insignificant terms at $P\leq0.05$. The adequacy of the model was inspected by examining residuals distribution and its independence. The main effect plot and interaction plot were employed to predict possible interactions. Finally, the response optimizer was applied to recognize the factor settings that optimize a TPA degradation percentage, cost, the sensitivity of factors, and desirability. Even-

Table 3. Factors and levels

Factors	Symbols	Levels	
		-1	+1
pH	A	5	9
Initial TPA conc. (ppm)	B	20	50
Catalyst amount (g L^{-1})	C	0.5	1.5
Ozone dosage (mg/h)	D	0.34	2.17

Archives of Hygiene Sciences
Qom University of Medical Sciences

tually, the efficiency of $MnFe_2O_4$/Willemite, $MnFe_2O_4$, and Willemite was compared under optimal conditions.

At any run, the TPA solution to a specific concentration, a particular pH, and a known amount of $MnFe_2O_4$/Willemite photo-catalyst was mixed in the tank. This solution was circulated in the reactor for 30 min in the absence of UV-A radiation to reach equilibrium. After homogenization, the radiation was started, and simultaneously, O_3 gas, created by an ozone generator, was injected from the bottom of the reactor by a spongy diffuser. The concentration of ozone in the gas phase was determined by the iodometric method, using 2% neutral buffered potassium iodide and sodium thiosulfate as a titrant [25]. The required samples were obtained at specified intervals, and the TPA concentration was measured by spectroscopy at 240 nm. The acidity was adjusted at the beginning of the experiments with dilute sodium hydroxide and sulfuric acid (about 0.1 M). Total Organic Carbon (TOC) was measured with a QBD1200 TOC laboratory analyzer (Hach Company). The TPA removal percentage was calculated by Equation 3 and recorded under experimental response. Where $[TPA]_0$ is the initial concentrations of TPA at the beginning of the photo-catalytic ozonation, and $[TPA]_t$ is the concentration of the TPA at the time t after the start of the process.

$$(3)\ Removal\ of\ TPA(\%)=\left(\frac{[TPA]_0-[TPA]_t}{[TPA]_0}\right)\times 100$$

3. Results

In the process of the mechanism of photo-degradation of TPA, $MnFe_2O_4$ semiconductor supported the Willemite absorbs photons from light (Figure 3). The photons which have energy equal (or more than) the photocatalyst band gaps, transfer electrons from the Valence Band (VB) to the Conduction Band CB). In this manner, holes and electrons are created in valance and conductive bonds, respectively. Then, the generated electrons

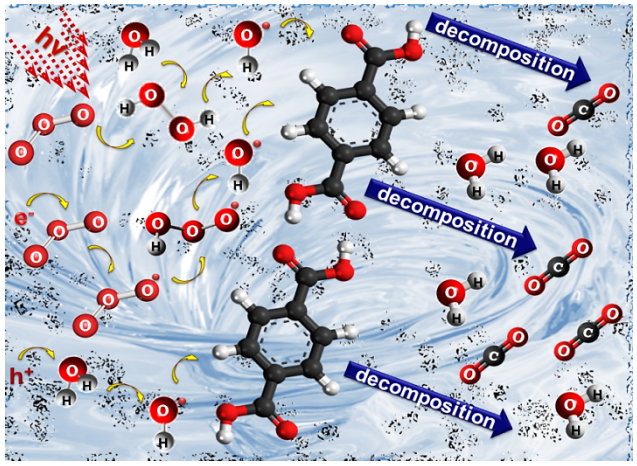

Terephthalic acid+O_3+UV-A $\xrightarrow{MnFe_2O_4/\ Willemite\ in\ CFBR\ reactor}$ CO_2+H_2O+Inorganic compounds

Figure 3. The mechanism of the photo-degradation of TPA in the experimental set-up

Archives of Hygiene Sciences
Qom University of Medical Sciences

Table 4. The full factorial design matrix

Run	Coded Variables				Response	
	O_3	Cat.	TPA	pH	Experimental	Predicted
1	1	-1	-1	1	92.0010	91.8603
2	-1	-1	1	1	61.9110	62.0031
3	0	0	0	0	68.2000	68.0974
4	-1	-1	1	-1	39.2000	39.3266
5	1	1	-1	1	98.0930	98.2695
6	-1	1	-1	1	92.7000	93.3318
7	-1	-1	-1	-1	50.0100	50.4590
8	1	-1	1	-1	50.6000	50.2859
9	1	1	-1	-1	53.7430	53.4195
10	1	1	1	1	86.9414	86.8101
11	-1	1	1	1	79.3420	79.2857
12	-1	1	-1	-1	65.7000	65.2868
13	1	1	1	-1	58.8000	59.1499
14	-1	-1	-1	1	79.1000	78.5040
15	0	0	0	0	68.1755	68.0974
16	1	-1	1	1	77.7789	77.9460
17	0	0	0	0	68.2030	68.0974
18	-1	1	1	-1	56.7000	56.6092
19	1	-1	-1	-1	46.6510	47.0103

Archives of Hygiene Sciences
Qom University of Medical Sciences

and holes migrate to other parts and the following the occurrence of reactions (Reactions 1-5).

(1) $MnFe_2O_4/Willemite+h\vartheta \rightarrow MnFe_2O_4/Willemite+(h^+ + e-)$

(2) $O_3+e- \rightarrow O_3\bullet-$

(3) $h^+ + H_2O \rightarrow H^+ + \bullet OH$

(4) $O_3\bullet- + H^+ \rightarrow HO_3\bullet-$

(5) $HO_3\bullet- \rightarrow \bullet OH+O_2$

Furthermore, hydroxyl radicals are created by the radiation of UV on ozone and hydrogen peroxide in solution (Reaction 6 and 7).

(6) $O_3+H_2O+hv \rightarrow H_2O_2+O_2$

(7) $H_2O_2+hv \rightarrow 2OH\bullet$

Finally, Hydroxyl radicals and ozone, attack organic matter. Subsequently, organic matter is oxidized and decomposed (Reactions 8-10) [26].

(8) $O_3 + R \rightarrow R_{ox}$

(9) $O_3+OH- \rightarrow OH\bullet+(O_2\bullet \leftrightarrow HO_2\bullet)$

Table 5. ANOVA data after removing insignificant factors

Source	df	Adj. SS	Adj. MS	F	P
Model	10	5165.75	516.57	2373.11	0.0001
Linear	4	4735.80	1183.95	5438.99	0.0001
pH	1	3796.51	3796.51	17440.91	0.0001
TPA	1	278.26	278.26	1278.31	0.0001
Cat.	1	561.30	561.30	2578.60	0.0001
O_3	1	99.73	99.73	458.14	0.0001
2-way interactions	5	395.1	79.00	362.93	0.0001
pH×TPA	1	127.22	127.22	584.44	0.0001
pH×O_3	1	118.69	118.69	545.24	0.0001
TPA×Cat.	1	6.03	6.03	27.68	0.001
TPA×O_3	1	72.20	72.20	331.70	0.0001
Cat.×O_3	1	70.87	70.87	325.59	0.0001
3-way interactions	1	34.94	34.94	160.49	0.0001
pH×TPA×O_3	1	34.94	34.94	160.49	0.0001
Error	8	1.74	0.22	-	
Lack-of-Fit	6	1.74	0.29	1274.97	0.071
Pure error	2	0.0001	0.0001		
Total	18	5167.49			

Archives of Hygiene Sciences
Qom University of Medical Sciences

df=Degree of Freedom; Adj.SS=Adjusted sum of square; Adj.MS=Adjusted mean of square; F=value on the F distribution P=probability value

(10) $OH\bullet + R\bullet \longrightarrow R_{ox}$

The percentages of TPA degradation for 19 sequential experiments regarding the influence of factors, the levels, and the combination of factors were applied for the execution of full factorial design (Table 4). The comparison of P-value of the main factors and interaction factors, choosing α-level of 0.05 indicated that TPA, pH, O_3, Cat., pH×TPA, pH×O_3, TPA×Cat., TPA×O_3, Cat.× O_3, and pH×TPA×O_3 were statistically significant. In other words, the mentioned terms were effective with %95 probability. Moreover, the P-value of the lack of Fits (0.071) was more than the selected α-value (0.05), reflecting that the model accurately fitted the data (Table 5).

The R^2 value emphasized that the model can explain 99.97% of the variance in TPA degradation yield. The adjusted R^2 was measured as 99.92 %. Both values signify that the model fitted the data well. R^2 prediction was computed as 99.68% for the new observations. The standard deviation of the residuals (S) was equal to 0.46656. This value reflected the standard distance of data from the regression line.

The regression coefficients were obtained by Equation 4 based on un-coded data. In this pattern, Deg% is the percentage of TPA degradation yield or response; pH, Cat., TPA, and O_3 are factors; Equation 4 represents the relationship between the percentage of TPA degradation and predictor variables. In this equation, the overall mean score was equal to 68.097, and the absolute value of the coefficient expresses the relative strength of each factor:

(4) $Deg\%=68.097+15.404pH-4.170TPA+5.923Cat.+2.97O_3-2820pH\times TPA+2.724p$

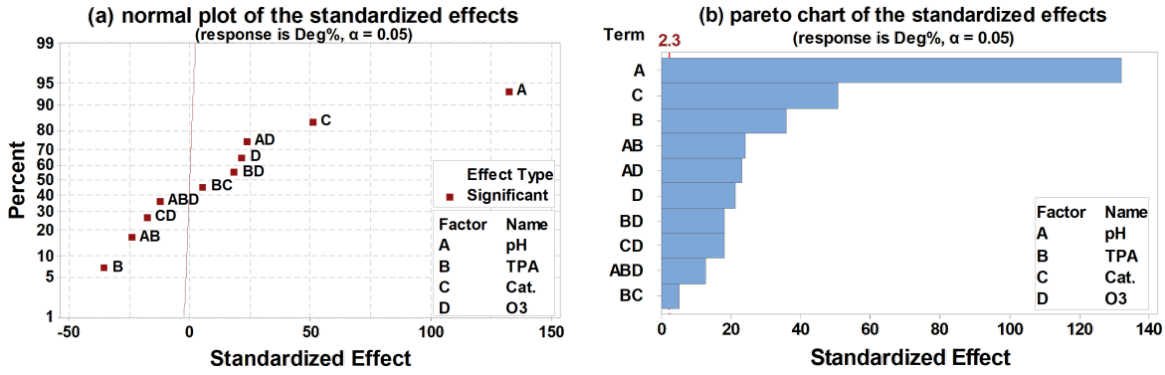

Figure 4. The normal plot of the standardized effects

A: Normal plot of the standardized effects; B: Pareto chart of the standardized effects.

$H \times O_3 + 0.614 TPA \times Cat. + 2.124 TPA \times O_3 - 2.105 Cat. \times O_3 - 1.478 pH \times TPA. \times O_3$

The normal plot of the standardized effects (Figure 4A) shows that all the main effects were significant. Besides, AB (pH by TPA conc.) and AD (pH by O3), as the interaction effects, presented the largest effect on the response, and BC (TPA by O3) provided the slightest effect on response. Furthermore, the normal plot proves that A, C, D, AD, BC, and BD positively impacted the response. In other words, the TPA degradation yields increase when the mentioned effects are altered from the low-level to the high levels.

Pareto chart of the standardized effects (Figure 4B) displays the ranking of effects; there exist 10 significant effects on the TPA elimination processes.

Residual plots were considered to check the assumptions of normality, constant variance, and randomness in the final model (Figure 5). The normal probability plot (Figure 5A) illustrates that the data were normally distributed, and outliers did not exist in the data. Ad-

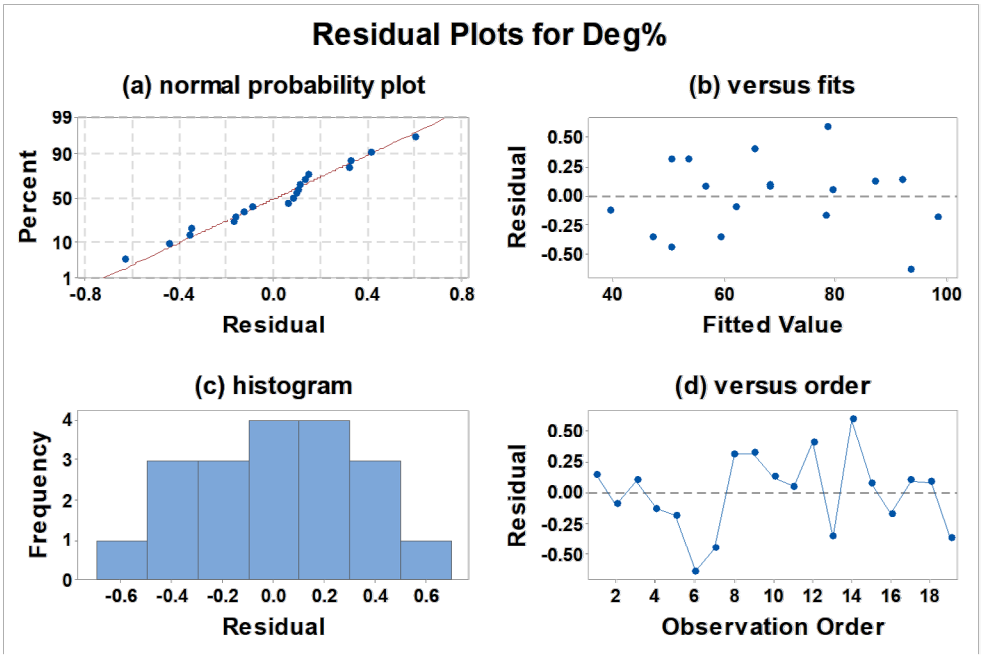

Figure 5. Residual plots for the percentage of degradation

A: The normal probability plot of residuals; B: Residuals versus fitted values; C: The histogram of the residuals; D: Residuals versus the order of the data.

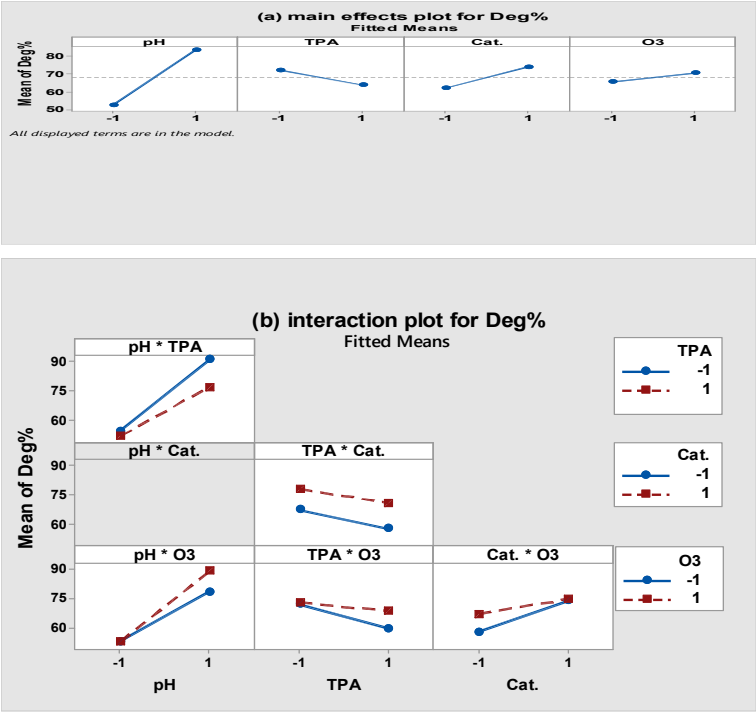

Figure 6. The magnitude of the main effect for pH

A: Main effects plot; and B: Interaction plot for percent of TPA degradation.

ditionally, residuals versus fitted values (Figure 5B) established no outlets, and the normality assumption of residuals was valid. In the histogram (Figure 5C), there was no distance between bars; thus, it signifies that outliers did not exist in the data. Residuals versus the order of the data (Figure 5D), specified no systematic effects in the data due to the time or order of data collection. The structure of Figure 5D acknowledges no correlation between the residuals. Thus, all mentioned interpretations confirmed that the ANOVA data (Table 5) were reliable and the model can predict TPA degradation yield within +/- 0.4665 with a 95% confidence level.

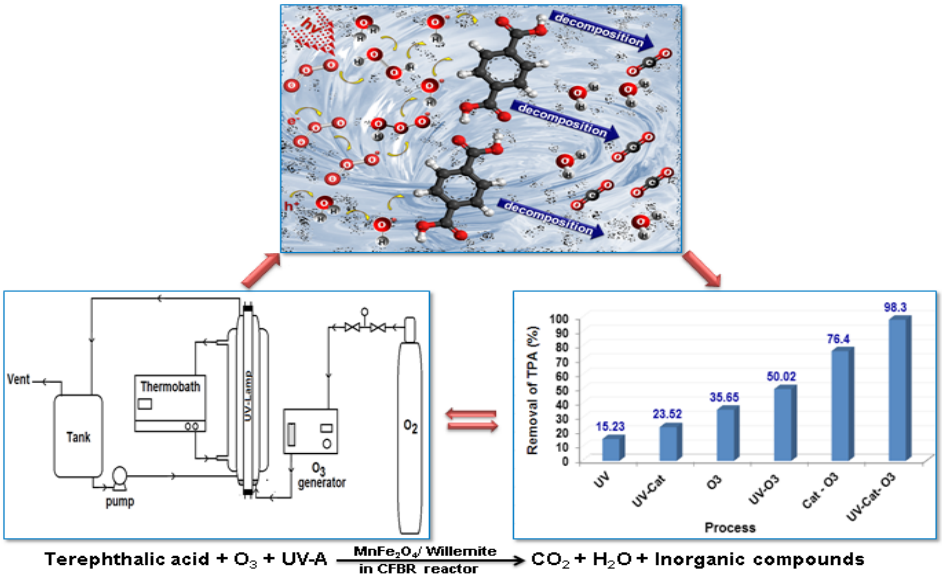

Figure 7. The percentage of TPA removal under different process

Table 6. The kinetic equations of TPA degradation in optimum conditions

Nanoparticles	Kinetic Equations	R^2	K_{app} (min^{-1}) Apparent Speed Constants
$MnFe_2O_4$/Willemite	Y=0.2707x-0.3723	0.997	0.2707
$MnFe_2O_4$	Y=0.0976x-0.1063	0.9933	0.0976

Archives of Hygiene Sciences
Qom University of Medical Sciences

Table 7. The Langmuir-Hinshelwood kinetic of TPA degradation in optimum conditions

Nanoparticles	Kinetic Equations	R^2	KLH (ppm min^{-1})	K_{add} (ppm^{-1})
$MnFe_2O_4$/Willemite	Y= 0.2681x-5.3821	0.985	3.729	0.051

Archives of Hygiene Sciences
Qom University of Medical Sciences

The settings that maximize degradation of TPA were determined by target parameters (goal=100 i.e., target, lower boundary=39.2, & upper boundary=100) in response optimizer for each response. The best-operating conditions which maximized the sensitivity of factors and desirability were obtained equal to 9, 20 ppm, 1.5 g/L, and 2.17 mg/h for pH, TPA, Cat., and O_3, in sequence. The predicted value for photo-catalyst efficiency and desirability, based on the best factor levels, equaled 98.2695% and 0.97168, respectively.

The magnitude of the main effect for pH indicated the greater effect of it, compared to the other variables. Besides, the main effects plot proves that pH, Cat., and O_3 positively affected the response. Furthermore, TPA adversely impacted the response (Figure 6A). The interaction plot for the percentage of TPA degradation (Figure 6B) manifested several interactions, as lines are not parallel to each other.

The plot indicated the increase in the degradation of TPA (Deg%) while the amount of TPA changes from 50 ppm to 20 ppm depending on the extent of ozone. While ozone is low (dashed line), the change in degradation is more than the time when ozone is high (straight line). Additionally, enhanced degradation of TPA (Deg%), as moving from the low to the high level of catalyst, is greater while the ozone is lower than (straight line) the time when it is high (dashed line).

Moreover, the interaction plot indicates that the increase in the degradation of TPA (Deg%) when the pH changes from low to high depending on the amount of TPA and ozone. When the amount of TPA is high, the alternation in degradation is less than low TPA. Moreover, when O_3 dosage is high, the change in degradation is more than low O_3 conditions.

To compare different processes, the TPA degradation experiments were performed by UV, UV-Cat., O_3, UV-O_3, Cat.-O_3, and UV-Cat.-O_3, separately. The relevant results suggested that the UV-Cat.-O_3 process presented a higher efficiency (Figure 7). The percentage of TPA removal in the UV-Cat.-O_3 process indicated that $MnFe_2O_4$/Willemite contributes to ozone decomposition and radicals generation.

To investigate the kinetics of TPA degradation, the experiments were performed by synthesized photo-catalysts in optimum conditions. Then, experimental data were fitted with Equation 5. Where A0 and A are the maximum absorptions at maximum absorption wavelength before light exposure and the maximum absorption at time t, respectively. Moreover, k represents the rate constant.

$$(5)\ Ln\frac{A_0}{A}=kt$$

The kinetic equations (Table 6) reveal that the TPA photo-degradation reactions by $MnFe_2O_4$/Willemite and $MnFe_2O_4$ catalyst approximately are the pseudo-first-order kinetics. Comparing apparent speed constants (K_{app}) of kinetic equations clarified that $MnFe_2O_4$/Willemite presented the most efficiency in the TPA photo-catalytic degradation processes. The increase in the efficiency of catalyst can be due to fixing $MnFe_2O_4$ on Willemite. The effective surface of the catalyst and the number of active sites was increased by fixing $MnFe_2O_4$ on the surface of Willemite.

To gather more evidence, a modified Langmuir-Hinshelwood (L-H) equation was applied (Equation 6). Where k_{add}, k_{LH}, and k are the apparent Langmuir adsorption constant, the apparent maximum photo-catalytic degradation rate, and the pseudo-first-order kinetic constant (derived from Equation 4), respectively. C0

represents the initial concentration of TPA. L-H kinetic parameters were obtained corresponding to Table 7.

$$(6)\ \frac{1}{k}=\frac{1}{k_{add}k_{LH}}+\frac{C_0}{k_{LH}}$$

After performing 5 successive experiments under optimal conditions with depreciated NPs of $MnFe_2O_4$/Willemite, comparing the degradation percentage of those experiments revealed that the catalyst provided desirable efficiency and repeatability (Deg% 98.02, 97.5, 97.04, 96.78, 96.53).

4. Discussion

The contamination of water by aromatic compounds, like TPA, is among the greatest problems. Therefore, in this research, an applied, affordable, and efficient method was presented for the degradation of TPA. The high yield of the TPA photo-degradation process applying O_3/$MnFe_2O_4$/Willemite as photo-catalytic ozonation under UV irradiation process corroborated the high efficiency of the employed method.

The study data disclosed that DOE, using full factorial design, is the best technique to ascertain the efficiency of O_3/$MnFe_2O_4$/Willemite, to define influential factors, to minimize response variability, and to affect the uncontrollable variables, to reduce reaction time and total cost; consequently, to optimize response. In this regard, the TPA degradation process was successfully modeled employing a full factorial methodology. of the obtained ANOVA data were reliable; thus, the model can predict TPA degradation yield within +/-0.46656 and a 95% confidence level. The model with R^2 of 99.97%, Adj. R^2 of 99.92% and Pred. R^2 of 99.68% fitted the data well. Additionally, according to optimized results, the best level for operation factors of pH, TPA, Cat., and O_3 was obtained equal to 9, 20 ppm, 1.5 g/L, and 2.17 mg/h, in sequence. According to optimal conditions, the results of testing the catalyst indicated that the model is suitable and the photo-catalyst is efficient. In addition, the operation factors provided the highest sensitivity due to the efficiency of 98.2695% and the desirability of 0.97168.

5. Conclusion

TPA decomposition kinetics was determined pseudo-first-order. Furthermore, the repeatability of the results of the 5 tests of TPA degradation using the depreciated photo-catalyst of $MnFe_2O_4$/Willemite and its constant value indicated that the photo-catalyst is considerably reusable and economic. Therefore, based on the evidence, implementing this catalyst is recommended to TPA producer companies. Moreover, developing studies and using $MnFe_2O_4$/Willemite photo-catalyst in the removal of other aromatic pollutants are recommended.

Ethical Considerations

Compliance with ethical guidelines

This article is a meta-analysis with no human or animal sample.

Funding

This research did not receive any specific grant from funding agencies in the public, commercial, or not-profit sectors.

Authors' contributions

All authors equally contributed to preparing this article.

Conflict of interest

The authors declared no conflicts of interest.

Acknowledgments

The authors gratefully appreciate Islamic Azad University, Arak branch for supporting the researchers.

References

[1] Damerau K, Patt AG, van Vliet OPR. Water saving potentials and possible trade-offs for future food and energy supply. Global Environmental Change. 2016; 39:15-25. [DOI:10.1016/j.gloenvcha.2016.03.014]

[2] Díaz A, Katsarava R, Puiggalí J. Synthesis, properties and applications of biodegradable polymers derived from diols and dicarboxylic acids: From polyesters to poly(ester amide)s. International Journal of Molecular Sciences. 2014; 15(5):7064-123. [DOI:10.3390/ijms15057064]

[3] Thiruvenkatachari R, Kwon TO, Jun JC, Balaji S, Matheswaran M, Moon IS. Application of several advanced oxidation processes for the destruction of Terephthalic Acid (TPA). Journal of hazardous materials. 2007; 142(1-2):308-14. [DOI:10.1016/j.jhazmat.2006.08.023]

[4] Kricheldorf HR, Schmidt B. New polymer syntheses. 69. Polyamides derived from deuterated terephthalic acid or phenoxyterephthalic acid. Macromolecules. 1992; 25(23):6090-4. [DOI:10.1021/ma00049a002]

[5] Cui L, Shi Y, Dai G, Pan H, Chen J, Song L, et al. Modification of N-Methyl-N-Nitrosourea initiated bladder carcinogenesis in Wistar rats by terephthalic acid. Toxicology and Applied Pharmacology. 2006; 210(1-2):24-31. [DOI:10.1016/j.taap.2005.06.008]

[6] Zhang XX, Sun SL, Zhang Y, Wu B, Zhang ZY, Liu B, et al. Toxicity of purified terephthalic acid manufacturing wastewater on reproductive system of male mice (Mus muscu-

lus). Journal of Hazardous Materials. 2010; 176(1-3):300-5. [DOI:10.1016/j.jhazmat.2009.11.028]

[7] Prasse C, Stalter D, Schulte-Oehlmann U, Oehlmann J, Ternes TA. Spoilt for choice: A critical review on the chemical and biological assessment of current wastewater treatment technologies. Water Research. 2015; 87:237-70. [DOI:10.1016/j.watres.2015.09.023]

[8] Mehta D, Mazumdar S, Singh SK. Magnetic adsorbents for the treatment of water/wastewater-a review. Journal of Water Process Engineering. 2015; 7:244-65. [DOI:10.1016/j.jwpe.2015.07.001]

[9] Rajasulochana P, Preethy V. Comparison on efficiency of various techniques in treatment of waste and sewage water-a comprehensive review. Resource-Efficient Technologies. 2016; 2(4):175-84. [DOI:10.1016/j.reffit.2016.09.004]

[10] Qu X, Alvarez PJJ, Li Q. Applications of nanotechnology in water and wastewater treatment. Water Research. 2013; 47(12):3931-46. [DOI:10.1016/j.watres.2012.09.058]

[11] Kunduru KR, Nazarkovsky M, Farah Sh, Pawar RP, Basu A, Domb AJ. Nanotechnology for water purification: Applications of nanotechnology methods in wastewater treatment. In: Grumezescu AM, editor. Water Purification. London: Academic Press; 2017. pp. 33-74 [DOI:10.1016/B978-0-12-804300-4.00002-2]

[12] Cushing BL, Kolesnichenko VL, O'Connor CJ. Recent advances in the liquid-phase syntheses of inorganic nanoparticles. Chemical Reviews. 2004; 104(9):3893-946. [DOI:10.1021/cr030027b]

[13] Takesue M, Hayashi H, Smith Jr RL. Thermal and chemical methods for producing zinc silicate (willemite): A review. Progress in Crystal Growth and Characterization of Materials. 2009; 55(3-4):98-124 [DOI:10.1016/j.pcrysgrow.2009.09.001]

[14] Myers RH, Montgomery DC, Vining GG, Borror CM, Kowalski SM. Response surface methodology: A retrospective and literature survey. Journal of Quality Technology. 2004; 36(1):53-77. [DOI:10.1080/00224065.2004.11980252]

[15] Thiruvenkatachari R, Ouk Kwon T, Shik Moon I. Degradation of phthalic acids and benzoic acid from terephthalic acid wastewater by advanced oxidation processes. Journal of Environmental Science and Health, Part A. 2006; 41(8):1685-97. [DOI:10.1080/10934520600754136]

[16] Lin XH, Lee SN, Zhang W, Li SFY. Photocatalytic degradation of terephthalic acid on sulfated titania particles and identification of fluorescent intermediates. Journal of Hazardous Materials. 2016; 303:64-75. [DOI:10.1016/j.jhazmat.2015.10.025]

[17] Fuentes I, Rodriguez JL, Tiznado H, Romo-Herrera JM, Chairez I, Poznyak T. Terephthalic acid decomposition by photocatalytic ozonation with V_xO_y/ZnO under different UV-A LEDs distributions. Chemical Engineering Communications. 2020; 207(2):263-77. [DOI:10.1080/00986445.2019.1581617]

[18] Shafaei A, Nikazar M, Arami M. Photocatalytic degradation of terephthalic acid using titania and zinc oxide photocatalysts: Comparative study. Desalination. 2010; 252(1-3):8-16. [DOI:10.1016/j.desal.2009.11.008]

[19] Yuefeng Ch, Hui W, Mingjuan H, Guofeng G. Photocatalytic degradation of organic pollutants in purified terephthalic acid wastewater with activated carbon supported titanium dioxide. Paper presented at: 2009 International Conference on Energy and Environment Technology. 16-18 October 2009; Guilin, China. [DOI:10.1109/ICEET.2009.397]

[20] Fuentes I, Rodríguez JL, Poznyak T, Chairez I. Photocatalytic ozonation of terephthalic acid: A by-product-oriented decomposition study. Environmental Science and Pollution Research. 2014; 21(21):12241-8. [DOI:10.1007/s11356-014-3176-1]

[21] Yener HB, Helvacı ŞŞ. Visible light photocatalytic activity of rutile TiO_2 fiber clusters in the degradation of terephthalic acid. Applied Physics A. 2015; 120(3):967-76. [DOI:10.1007/s00339-015-9263-4]

[22] Zaitseva NA, Onufrieva TA, Barykina JA, Krasnenko TI, Zabolotskaya EV, Samigullina RF. Magnetic properties and oxidation states of manganese ions in doped phosphor Zn_2SiO_4: Mn. Materials Chemistry and Physics. 2018; 209:107-11. [DOI:10.1016/j.matchemphys.2018.01.071]

[23] Bharathi S, Nataraj D, Mangalaraj D, Masuda Y, Senthil K, Yong K. Highly mesoporous α-Fe_2O_3 nanostructures: Preparation, characterization and improved photocatalytic performance towards Rhodamine B (RhB). Journal of Physics D: Applied Physics. 2009; 43(1):015501. [DOI:10.1088/0022-3727/43/1/015501]

[24] Amighian J, Mozaffari M, Nasr B. Preparation of nano-sized manganese ferrite ($MnFe_2O_4$) via coprecipitation method. Physica Status Solidic. 2006; 3(9):3188-92. [DOI:10.1002/pssc.200567054]

[25] Rakness K, Gordon G, Langlais B, Masschelein W, Matsumoto N, Richard Y, et al. Guideline for measurement of ozone concentration in the process gas from an ozone generator. Ozone: Science & Engineering. 1996; 18(3):209-29. [DOI:10.1080/01919519608547327]

[26] Wang JL, Xu LJ. Advanced oxidation processes for wastewater treatment: Formation of hydroxyl radical and application. Critical Reviews in Environmental Science and Technology. 2012; 42(3):251-325. [DOI:10.1080/10643389.2010.507698]

This Page Intentionally Left Blank